Arteriosclerosis, Thrombosis, and Vascular Biology

BASIC SCIENCES

IL11 (Interleukin-11) Causes Emphysematous Lung Disease in a Mouse Model of Marfan Syndrome

Benjamin Ng, Chen Xie, Liping Su, Fathima F. Kuthubudeen, Xiu-Yi Kwek, Daryl Yeong, Chee Jian Pua, Stuart A. Cook*, Wei-Wen Lim*

BACKGROUND: Marfan Syndrome (MFS) is an inherited connective tissue disorder caused by mutations in the FBN1 (fibrillin-1) gene. Lung abnormalities are common in MFS, but their pathogenesis is poorly understood. IL11 (interleukin-11) causes aortic disease in a mouse model of MFS and was studied here in the lung.

METHODS: We examined histological and molecular phenotypes in the lungs of *Fbn1*$^{C1041G/+}$ mice (mouse model of Marfan Syndrome [mMFS]), an established mouse model of MFS. To identify IL11-expressing cells, we used immunohistochemistry on lungs of 4- and 16-week-old *Fbn1*$^{C1041G/+}$:*Il11*$^{EGFP/+}$ reporter mice. We studied the effects of IL11 inhibition by RT-qPCR, immunoblots and histopathology in lungs from genetic or pharmacologic models: (1) 16-week-old IL11 receptor (IL11RA) knockout mMFS mice (*Fbn1*$^{C1041G/+}$:*Il11ra1*$^{-/-}$ mice) and (2) in mMFS mice administered IgG control or interleukin-11 receptor antibodies twice weekly from 4 to 24 weeks of age.

RESULTS: mMFS lungs showed progressive loss and enlargement of distal airspaces associated with increased proinflammatory and profibrotic gene expression as well as matrix metalloproteinases 2, 9, and 12. IL11 was increased in mMFS lungs and localized to smooth muscle and endothelial cells in young mMFS mice in the *Fbn1*$^{C1041G/+}$:*Il11*$^{EGFP/+}$ reporter strain and in fibroblasts, in older mice. In mMFS mice, genetic (*Fbn1*$^{C1041G/+}$:*Il11ra1*$^{-/-}$) or pharmacologic (anti-interleukin-11 receptor) inhibition of IL11 signaling reduced lung emphysema, fibrosis, and inflammation. This protective effect was associated with reduced pathogenic ERK1/2 signaling and lower metalloproteinase 2, 9, and 12 expression.

CONCLUSIONS: IL11 causes lung disease in mMFS. This reveals a shared IL11-driven disease mechanism in lung and aorta in MFS and suggests inhibition of IL11 signaling as a holistic approach for treating multiorgan morbidity in MFS.

GRAPHIC ABSTRACT: A graphic abstract is available for this article.

Key Words: fibrosis ■ interleukin-11 ■ Marfan syndrome ■ pathology ■ pulmonary emphysema

Marfan syndrome (MFS) is an autosomal dominant genetic disorder caused by mutations in the fibrillin-1 (*FBN1*) gene resulting in connective tissue abnormalities that leads to bone overgrowth, scoliosis, ectopia lentis, and aortic aneurysm. In MFS, the primary cause of morbidity and mortality is due to thoracic aortic aneurysm and rupture.[1,2] Pulmonary disease in patients with MFS, which can develop as early as infancy, is common and mutations in FBN1 (fibrillin-1) are known to disrupt the microfibrillar assembly required for elastin deposition, to reduce lung elasticity and recoil.[3,4] While improvements in the diagnosis and treatment of MFS aortopathy has led to near-normal life expectancy in MFS patients,[5] pulmonary disease still causes disability and affects quality of life.[6,7] Pneumothorax commonly occurs in MFS patients and only 1 in 3 patients with MFS have normal pulmonary function.[8]

Correspondence to: Stuart A. Cook, National Heart Research Institute Singapore, National Heart Centre Singapore, 169609, Singapore, Email stuart.cook@duke-nus.edu.sg; or Wei-Wen Lim, National Heart Research Institute Singapore, National Heart Centre Singapore, 169609, Singapore, Email lim.wei.wen@nhcs.com.sg
*S.A. Cook and W.-W. Lim contributed equally.
Supplemental Material is available at https://www.ahajournals.org/doi/suppl/10.1161/ATVBAHA.122.318802.
For Sources of Funding and Disclosures, see page 752.

Arterioscler Thromb Vasc Biol is available at www.ahajournals.org/journal/atvb

Nonstandard Abbreviations and Acronyms

ACTA2	actin alpha 2
AGER	advanced glycosylation end-product specific receptor
ECM	extracellular matrix
EGFP	enhanced green fluorescent protein
ERK	extracellular signal regulated kinase
FBN1	fibrillin-1
IL11	interleukin-11
IL11RA	interleukin-11 receptor
MFS	Marfan syndrome
MLI	mean linear intercept
mMFS	mouse model of Marfan Syndrome
MMP	matrix metalloproteinase
PDGFRA	platelet-derived growth factor receptor alpha
SFTPC	surfactant protein C
TGFβ	transforming growth factor beta
WT	wild type

Highlights

- The present study investigated whether the inhibition of IL11 (interleukin-11) signaling reduces lung disease in a mouse model of Marfan Syndrome.
- In Marfan syndrome IL11 is upregulated early in pulmonary airways and vasculature before being expressed in parenchymal fibroblasts, later in disease.
- Inhibition of IL11 signaling either by genetic deletion of the IL11 receptor or the use of a neutralizing IL11RA antibody prevents pulmonary fibrosis, inflammation, and emphysema in a mouse model of Marfan Syndrome.
- Therapeutic inhibition of IL11, imminent in clinical trials, may be an effective intervention for preventing both lung and aortic disease in Marfan patients.

Mouse models have been informative in the study of MFS lung disease, although many exhibit high postnatal mortality due to aortic disease. Mice with null mutations in *Fbn1* (*Fbn1*$^{mgN/mgN}$) have alveolar space enlargement and pulmonary blebs.[9] Mice hypomorphic for Fbn1 (*Fbn1*$^{mg\Delta/mg\Delta}$) express ≈10% of normal fibrillin-1 levels also exhibit distal airspace enlargement.[10–12] The *Fbn1*$^{mgR/mgR}$ mouse,[13] expresses ≈20% of normal fibrillin-1 and has a similar lung pathology to that seen in human emphysema.[11,12] Fibrillin-1 is known to regulate the bioavailability of TGFβ (transforming growth factor beta),[14] and administration of a neutralizing transforming growth factor beta (TGFβ) antibody to pregnant *Fbn1*$^{mg\Delta/+}$ dams inhibits airspace enlargement in *Fbn1*$^{mg\Delta/mg\Delta}$ pups.[15] This suggest a pathogenic effect of TGFβ for lung disease in MFS.

The *Fbn1*$^{C1041G/+}$ mouse model of MFS (mMFS) is perhaps the most widely studied and faithful model of human MFS and recapitulates many of the skeletal, aortic, and pulmonary pathologies seen in human MFS, while having a long lifespan.[16,17] mMFS mice develop early defects in lung elastance, unrelated to extracellular matrix stiffness, and progressive airspace enlargement.[17] In this model, the MMP (matrix metalloproteinase) 2 and 9 contribute to elastin degradation and are important in disease pathology, not dissimilar to the role of MMP2/9 in MFS aortic disease.[18–20] Treatment of mMFS mice with the angiotensin II type I receptor blocker losartan reduces distal airspace dilatation by indirectly inhibiting TGFβ-dependent ERK1/2 signaling, implicating noncanonical TGFβ signaling in MFS lung pathology.[21,22]

IL11 (interleukin-11) is a principal transcriptional target for TGFβ-driven SMAD activity and is profibrotic and proinflammatory.[23,24] We recently showed that IL11 levels are increased in vascular smooth muscle cells in the aortas of mMFS mice where it contributes to aortopathy.[25,26] In the current study, we determine the expression of IL11 in the mMFS lung by western blotting and in an IL11:EGFP (enhanced green fluorescent protein) reporter strain and define the effects of genetic or therapeutic inhibition of IL11 signaling on lung pathobiology in mMFS.

MATERIALS AND METHODS

Data Availability

The Major Resources Table, uncropped Western blots, source datafile with exact *P* values are available in the Supplemental Material. The authors declare that data supporting the study findings are included in the article and the supporting files.

Study approval

The study was carried out in compliance with the recommendations in the Guidelines on the Care and Use of Animals for Scientific Purposes of the National Advisory Committee for Laboratory Animal Research (NACLAR). All experimental procedures (2019/SHS/1481 and 2019/SHS/1483) were approved by the SingHealth Institutional Animal Care and Use Committee.

Animal studies

All mice were from a C57BL/6J genetic background, bred and housed in individually vented cages under ABSL-2 conditions in the SingHealth Experimental Medicine Centre and provided standard laboratory diet (SF00-100; Specialty Feeds) and water ad libitum. *Fbn1*$^{C1041G/+}$ (mMFS) mice were purchased from Jackson Laboratories (012885).[16] Colony maintenance was carried out as highlighted in the Major Resources Table. Notably, infertility of *Il11ra1*$^{-/-}$ female mice posed certain challenges in the breeding design. Mice were sacrificed at their respective endpoint studies by vital organs removal under

deep anaesthesia with ketamine (100 mg/kg; IP) and xylazine (10 mg/kg; IP). Depth of sedation was checked periodically for paw- and tail-pinch reflexes. In all experiments, both sexes were used in keeping with previous studies of mMFS, providing a sex-balanced experimental design. Aortic investigations in these models have been presented elsewhere.[25]

IL11-EGFP Reporter Marfan Mice

Fbn1$^{C1041G/+}$ mice were bred with *Il11*$^{EGFP/+}$ mice[27] to generate hybrid *Fbn1*$^{C1041G/+}$ (mMFS):*Il11*$^{EGFP/+}$ mice. Age-matched *Fbn1*$^{+/+}$ (wild-type [WT]):*Il11*$^{EGFP/+}$ littermates were designated controls. Four- or 16-week-old mice were sacrificed, and the left lung lobes were analysed by immunofluorescence staining.

IL11RA KO Marfan Mice

Fbn1$^{C1041G/+}$ mice were bred with constitutive *Il11ra1*$^{-/-}$ knockout mice[23] in ≥2 rounds of hybrid crossings to generate *Fbn1*$^{C1041G/+}$:*Il11ra1*$^{-/-}$ (mMFSxKO) mice. The lungs of 16-week-old littermates and cousin lines were assessed for the 4 groups: *Fbn1*$^{+/+}$, *Fbn1*$^{C1041G/+}$, *Fbn1*$^{C1041G/+}$:*Il11ra1*$^{-/-}$, and *Il11ra1*$^{-/-}$ mice.

Antibody Treatment

Fbn1$^{C1041G/+}$ littermates were batch randomized to either 20 mg/kg of anti-interleukin-11 receptor (IL11RA; X209 clone) or isotype control IgG (11E10) twice a week from 4 to 24 weeks of age for terminal sacrifice. WT littermates were designated controls for comparison.

X209 Biodistribution in the Lung

C57BL/6J mice (10–12 weeks old) were retro-orbitally injected (left eye) with 100 µL of freshly radiolabelled ^{125}I-X209 (5 µCi, 2.5 µg) in PBS as previously described.[28] Lung tissues were harvested at the following time points: 1, 4 hours, 1, 3, 7, 14, 21 days post-injection. The radioactivity contents were measured using a gamma counter (2480 Wizard2; Perkin Elmer, Rockford, IL) with decay-corrections (100X dilution of 100 µL dose). The measured radioactivity was normalized to % injected dose/g tissue.

RT-qPCR

Total RNA was extracted from snap-frozen right lung superior lobe homogenates using RNAzol RT (Sigma-Aldrich) followed by Purelink RNA mini kit (Invitrogen) purification. The cDNA was synthesized using the iScript cDNA synthesis kit (Bio-Rad). Gene expression analysis was performed in duplicates using fast SYBR green (Qiagen) technology on the ViiA 7 real-time PCR system (Applied Biosystems). Expression data were normalized to Gapdh mRNA expression levels and fold-change was calculated using the $2^{-\Delta\Delta Ct}$ method.

Immunoblots

Western blot analysis was conducted on protein extracts from the mouse right inferior lung lobe. Snap-frozen tissues were homogenized and protein concentrations determined by the bicinchoninic acid method. Equal amounts of protein lysates were separated by SDS-PAGE and transferred onto a PVDF membrane. The membranes were blocked with 5% non-fat milk in Tris-buffered saline with 0.1% Tween for 1 hour at room temperature and incubated overnight at 4 °C with primary antibodies. Proteins were visualized using the ECL detection system with the appropriate secondary antibodies.

Hydroxyproline Assay

Total hydroxyproline content, a surrogate marker for tissue collagen concentration, was measured in the left lungs of mice using the Quickzyme Total Collagen assay kit as per manufacturer's instructions.

Histopathology

Animals were perfused-fixed with PBS followed by 10% neutral-buffered formalin through the left ventricle and effluent discharge from the right atria. The lungs were further fixed in fresh fixative for 24 to 48 hours, dehydrated, and paraffin-embedded. Five micrometer sections were stained with Masson's trichrome for collagen assessment, hematoxylin and eosin for nuclei analysis, and Verhoef Van Gieson stain for elastic fibres. Photomicrographs were randomly captured with non-overlapping fields by researchers (X.-Y.K. and D.Y.) blinded to the strain and treatment groups.

Immunohistochemistry

Tissue sections were deparaffinized, permeabilized, and antigen retrieved with Bull's Eye Decloaker. Slides were blocked for endogenous peroxidase followed by 3% BSA in PBS. Primary antibodies were incubated at 4 °C overnight and visualized with the ImmPRESS peroxidase kit. Five photomicrographs (20X magnification) were randomly captured in a lung section per mouse and manual cell count was performed with the Cell Counter plugin on ImageJ. Lung tissue area was quantified by thresholding on ImageJ. The cluster of differentiation molecule 68-positive cell counts per mm2 tissue area were averaged among 5 photomicrographs per mouse.

Immunofluorescence

Animals were perfused-fixed with 4% paraformaldehyde. The excised lungs underwent further fixation with 4% paraformaldehyde at 4 °C overnight, serial 15% to 30% sucrose dehydration for 48 hours and frozen in OCT compound. Lung sections were probed with primary antibodies at 4 °C overnight. Secondary antibodies were used for visualization. Autofluorescence was quenched with 0.1% Sudan Black B for 20 minutes. Photomicrographs were randomly captured by researchers (B.N. and F.F.K.) blinded to the strain and age groups. Percentage proportion of GFP^{+ve} cells colocalized to cell-type markers were reported per 5 fields, apart from AGER^{+ve} (advanced glycosylation end-product specific receptor) cells (percentage area) due to inability of delineating individual cells.

Lung Morphometry

Lung fibrosis was scored in 10 fields (10× magnification) per Masson's trichrome-stained section using the semiquantitative Ashcroft score as previously described.[29,30] To quantify mean linear intercept (MLI), we employed the validated semi-automated method for alveolar morphometry as established by Salaets et al.[31] Briefly, 20 fields (10× magnification) were randomly selected per HE-stained section, manual exclusion of non-parenchyma and alveolar exudates was performed on a semi-automated FIJI-macro plugin for counting of septal tissue points and intersections. Alveolar size measurements were analysed as previously established.[32] Alveolar airspace area was measured with the analyze particles tool. HE images were first converted to 8-bit and inverted, and alveolar spaces

identified with a preset of 50 μm² to infinity. Airways and vessels were excluded and ≥2000 alveoli were averaged per lung. Elastin area fraction was quantified by calculating the lung parenchyma area occupied by elastic fibres, like other publications.[33,34] Five random non-coinciding fields (20× magnification) per Verhoef-Van Gieson–stained section per mouse and analyzed on ImageJ. Thresholds for elastic fibres were established after contrast enhancement until fibres were identifiable as black bands. The elastin area was quantified by colour deconvolution using the ROI vector segmenting elastin, non-elastin and airspace (non-tissue) area followed by thresholding for elastin area and final expression as a percentage of total lung area (see Figure S1).

Statistics

Data are presented either as mean±SE or median±interquartile range, unless otherwise stated. Statistical analyses were conducted using GraphPad Prism (version 9.1.2). The robust regression and outlier removal tool (ROUT; Q=1%) was applied before analysis. Data normality assessed by Shapiro-Wilk test, and variance heteroscedasticity was assessed by *F*-test for *T*-test, Brown-Forsythe test for 1-way ANOVA, and Spearman rank correlation coefficient test of residuals for 2- or 3-way ANOVA where appropriate. Equal variance and normality of data determined whether non-linear variable transformation was performed and whether parametric or nonparametric tests were used. For normal distributed comparisons, 2-tailed unpaired Student *t*-test and 1-way ANOVA, with Sidak or Dunnett post hoc tests as appropriate. Welch's correction was applied to parametric tests when heteroscedasticity was identified. Non-parametric Kruskal-Wallis with Dunn multiple comparisons was conducted for non-normal data. Two-way ANOVA with Sidak multiple comparison was conducted to compare between *Fbn1*$^{C1041G/+}$ and *Il11ra1*$^{-/-}$ mouse genotypes. One-tailed non-parametric Mann-Whitney tests were performed at individual gene level for ECM (extracellular matrix) or inflammatory marker genes. Fisher's method was subsequently applied (metab R package, sum.log function) to combine *P* values (and corrected for multiple comparisons using Bonferroni with the stats R package, p.adjust function) to determine the activation of gene pathways in disease or mitigation of pathways with loss-of-function in IL11 signaling or antibody treatment. *P* values are presented corrected to 2 significant figures up to $P<0.0001$, with exact *P* values presented in the source data.

RESULTS

IL11 Is Upregulated in the Lung of *Fbn1*$^{C1041G/+}$ (mMFS) Mice

Early and progressive lung impairment has been previously reported in the mMFS mice and we studied lungs in mice across 4, 16, and 24 weeks of age.[17] Body, lung, and normalized lungs weights stratified for sex are presented in Figure S2A through S2D. We did not observe evidence of sexual dimorphism of normalized lung weights in the mMFS lungs (Figure S2D), which is apparent for aortic disease.[35] Normalized lung weights in mMFS mice were no different to age-matched WT controls but were significantly reduced in older mice (Figure 1A). By both hematoxylin and eosin (HE) and Masson's trichrome staining, parenchymal emphysema and fibrosis in mMFS lungs progressed with age (Figure 1B).

We assessed the expression of IL11 and its cognate receptor (IL11RA1) in lung tissues. By western blot analysis, IL11 was increased ≈2-fold ($P=0.0002$) in mMFS lungs as compared with WT controls (Figure 1C). By immunohistochemistry, we found that IL11 was notably expressed in airway epithelial cells and throughout the mMFS parenchyma but was not readily detected in the WT lung (Figure 1D). IL11RA was expressed widely and at a similar level in both WT and mMFS lungs (Figure 1D).

IL11 Is Upregulated in the Lung Vasculature in Young Marfan Syndrome Mice

To specifically identify the cells expressing IL11 in the lungs of mMFS, we crossed *Fbn1*$^{C1041G/+}$ (mMFS) mice to Il11-tagged EGFP reporter mice, generating *Fbn1*$^{+/+}$:*Il11*$^{EGFP/+}$ (WT:IL11-EGFP) and *Fbn1*$^{C1041G/+}$:*Il11*$^{EGFP/+}$ (mMFS:IL11-EGFP) mice. To define cell types, we used immunohistochemistry to colocalize EGFP expression with cell-specific markers: smooth muscle cell: ACTA2 (actin alpha 2); endothelial cell: cluster of differentiation 31; fibroblasts: PDGFRA (platelet-derived growth factor receptor-α); alveolar type 1 epithelial cell: AGER and alveolar type 2 epithelial cell: SFTPC (surfactant protein C; Figure 2).

In 4-week-old mMFS:IL11-EGFP mice, IL11 expression was limited to ACTA2+ SMCs in the pulmonary vasculature and airway smooth muscle with additional expression localised to CD31+ ECs throughout the lung (Figure 2). In older (16-week-old) mMFS:IL11-EGFP mice, IL11 expression was seen again in SMCs and ECs and additionally in fibroblasts. IL11 expression was seen in the lung epithelium but very rarely colocalized to alveolar type 2 epithelial cell or alveolar type 1 epithelial cell cells in both young and adult mMFS:IL11-EGFP mice. In contrast, EGFP signal was absent in WT lungs showing its upregulation to be specific to the mMFS genotype (Figure 2B through 2F). As such, in the Marfan lung, IL11 is first seen in vascular and airway smooth muscle and the endothelium and progresses with age to be expressed by airway and alveolar fibroblasts.

IL11 Causes Pulmonary Emphysema, Fibrosis, and Elastolysis in the Marfan Lung

To investigate the role of IL11 signaling in mMFS lung disease, we generated a hybrid cross of the *Fbn1*$^{C1041G/+}$

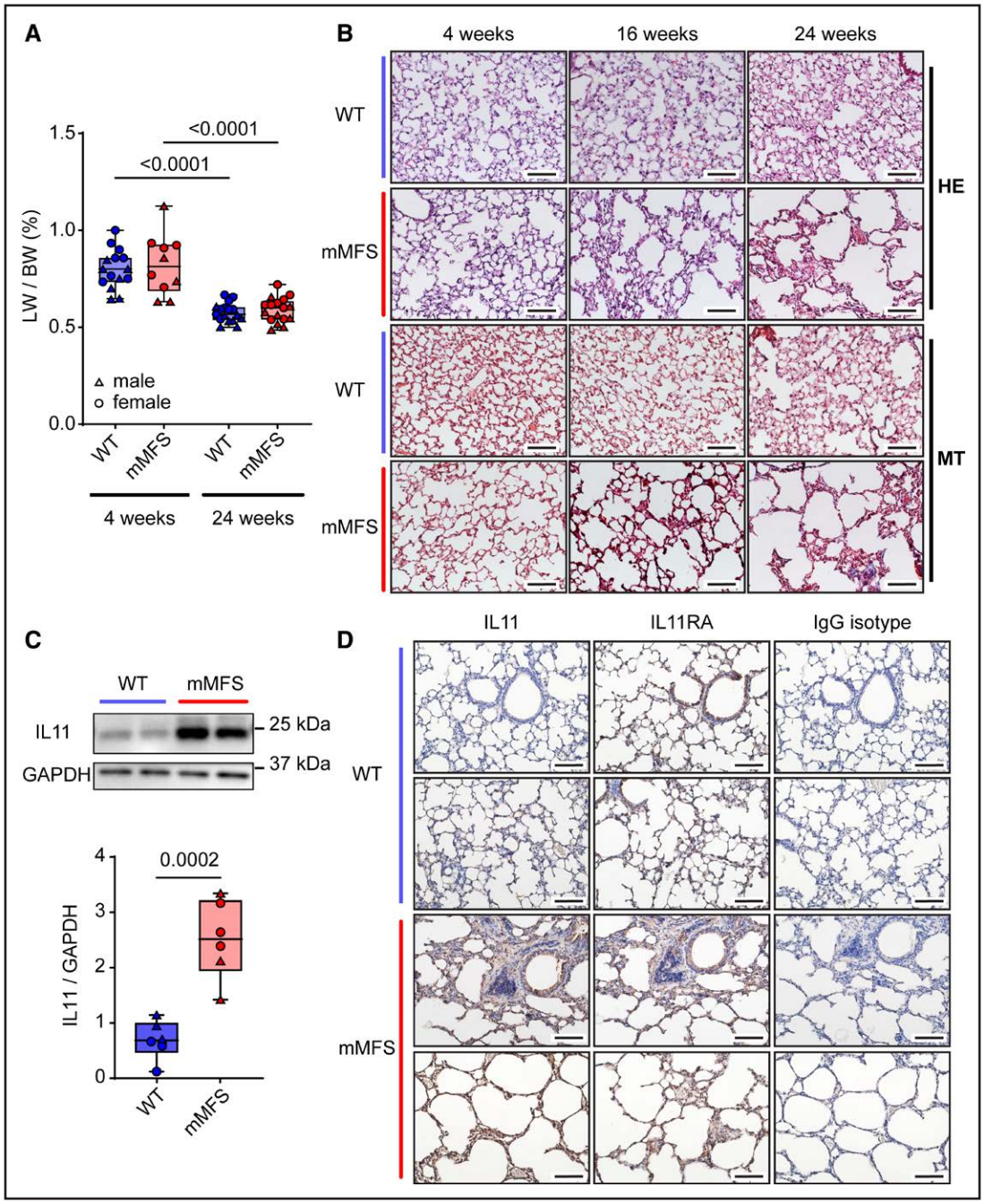

Figure 1. IL11 (interleukin-11) is upregulated in the diseased lungs of Marfan Syndrome mice.
A, Normalized lung-to-body weight ratio (LW/BW; %) is unaltered in age-matched mouse model of Marfan Syndrome (mMFS) mice compared with wild-type (WT) controls (4-week-old WT: n=7M, 8F; 4-week-old mMFS: n=5M, 5F; 24-week-old WT and mMFS: n=8M, 9F). **B**, Representative hematoxylin & eosin (HE) and Masson's trichrome (MT) stained lung cryosections demonstrate progressive emphysematous and fibrotic lung pathology in young 4-week-old to mature 24-week-old mMFS mice (n=3). **C**, Representative immunoblot and cumulative IL11 protein expression normalized to glyceraldehyde 3-phosphate dehydrogenase (GAPDH) is elevated in 24-week-old mMFS lungs compared with controls (n=3M, 3F). **D**, Representative immunohistochemistry in lung sections probed for IL11 and IL11 receptor (IL11RA) compared with an IgG isotype antibody in 24-week-old WT and mMFS lungs (n=3). Scale bar represents 50 μm. Data shown are expressed as median±interquartile range (IQR); whiskers denote minimum and maximum values. Statistical analysis was performed by 2-way ANOVA for age and strain factors with Sidak multiple comparisons (**A**) and unpaired Student 2-tailed *t*-test (**C**). Sexes are indicated as symbols for males (▲) and females (●).

(mMFS) mouse to the constitutive *Il11ra1*$^{-/-}$ knockout mouse, generating double mutant mMFS mice devoid of IL11RA1-mediated signaling (*Fbn1*$^{C1041G/+}$:*Il11ra1*$^{-/-}$; mMFSxKO). We studied these mice at 16 weeks of age, a time point when mMFS mice have established and stable lung pathology.[17] No evidence of sexual dimorphism in

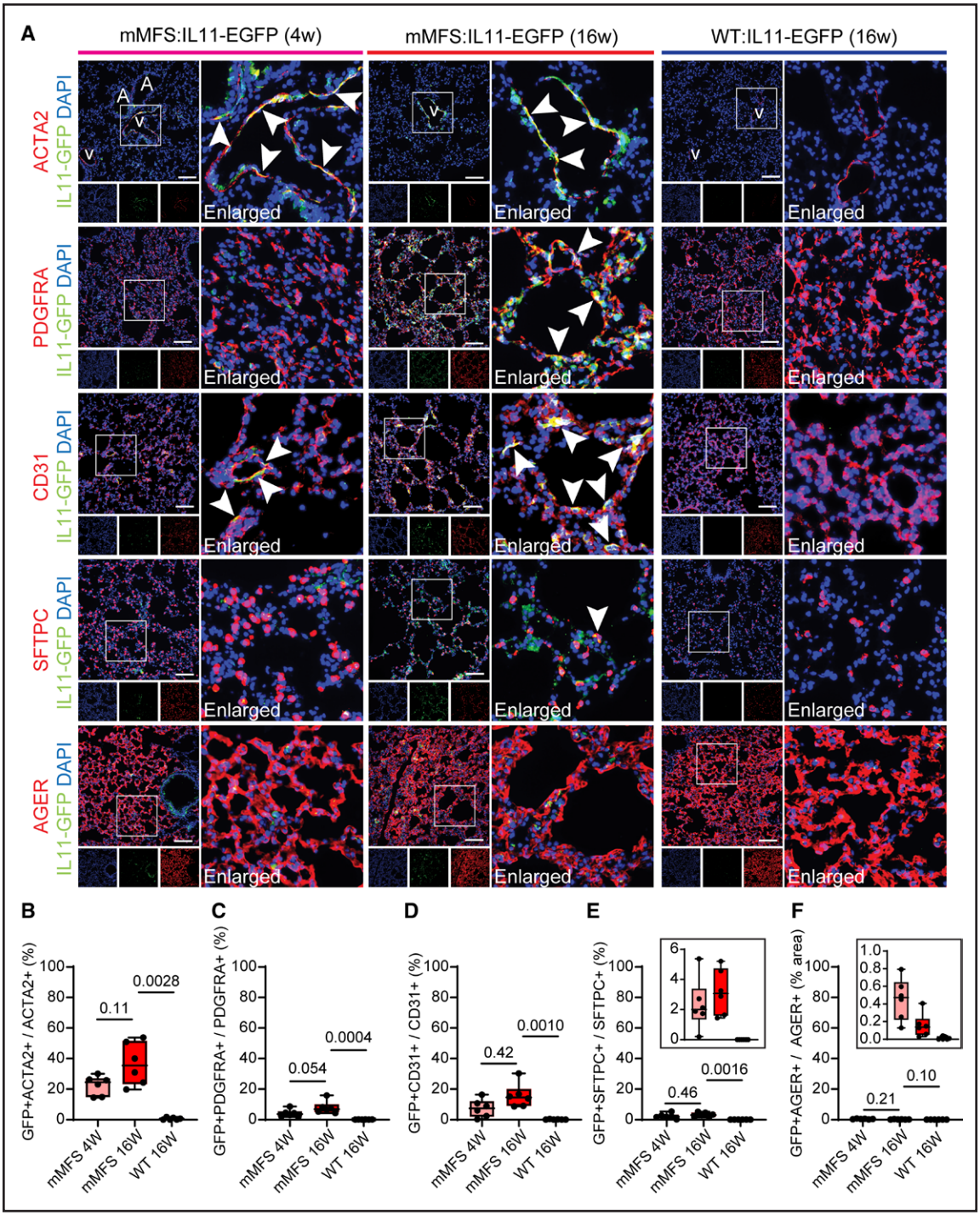

Figure 2. IL11 (interleukin-11) is upregulated in smooth muscle cells and endothelial cells in young Marfan mice as well as in fibroblasts in adult Marfan mice.

A, Immunofluorescence staining photomicrographs of lungs in WT:IL11-EGFP and mMFS:IL11-EGFP mice (n=6). ACTA2 (actin alpha 2; smooth muscle cells), PDGFRA (platelet-derived growth factor receptor-α; fibroblasts), CD31 (endothelial cells), SFTPC (surfactant protein C; AT2 cells), or AGER (advanced glycosylation end-product specific receptor; AT1 cells) in red, GFP in green and DAPI in blue. A and V represent airways and vessels in the distal lung regions in ACTA2 stained images respectively. Arrowheads indicate GFP+ cells that colocalize with the respective cell-specific markers. Scale bar represents 100 µm. **B** through **E**, Percentage proportion of GFP^{+ve} cells colocalized with ACTA2^{+ve} (**B**), PDGFRA^{+ve} (**C**), CD31^{+ve} (**D**), and SFTPC^{+ve} (**E**) cells, respectively. **F**, Percentage proportion of GFP^{+ve} area with respect to total AGER^{+ve} area. Inserts in **E** and **F** denote the extended *y*-axis for the 3 groups. Data shown are expressed as median±IQR; whiskers denote minimum and maximum values. Statistical analysis was performed by Welch 1-way ANOVA with Dunnet multiple comparisons (**B**), ordinary 1-way ANOVA with Dunnet multiple comparisons (**C** and **E**), and Kruskal-Wallis with Dunn multiple comparisons (**D** and **F**) against the 16-week-old mMFS group.

 Arterioscler Thromb Vasc Biol. 2023;43:739–754. DOI: 10.1161/ATVBAHA.122.318802

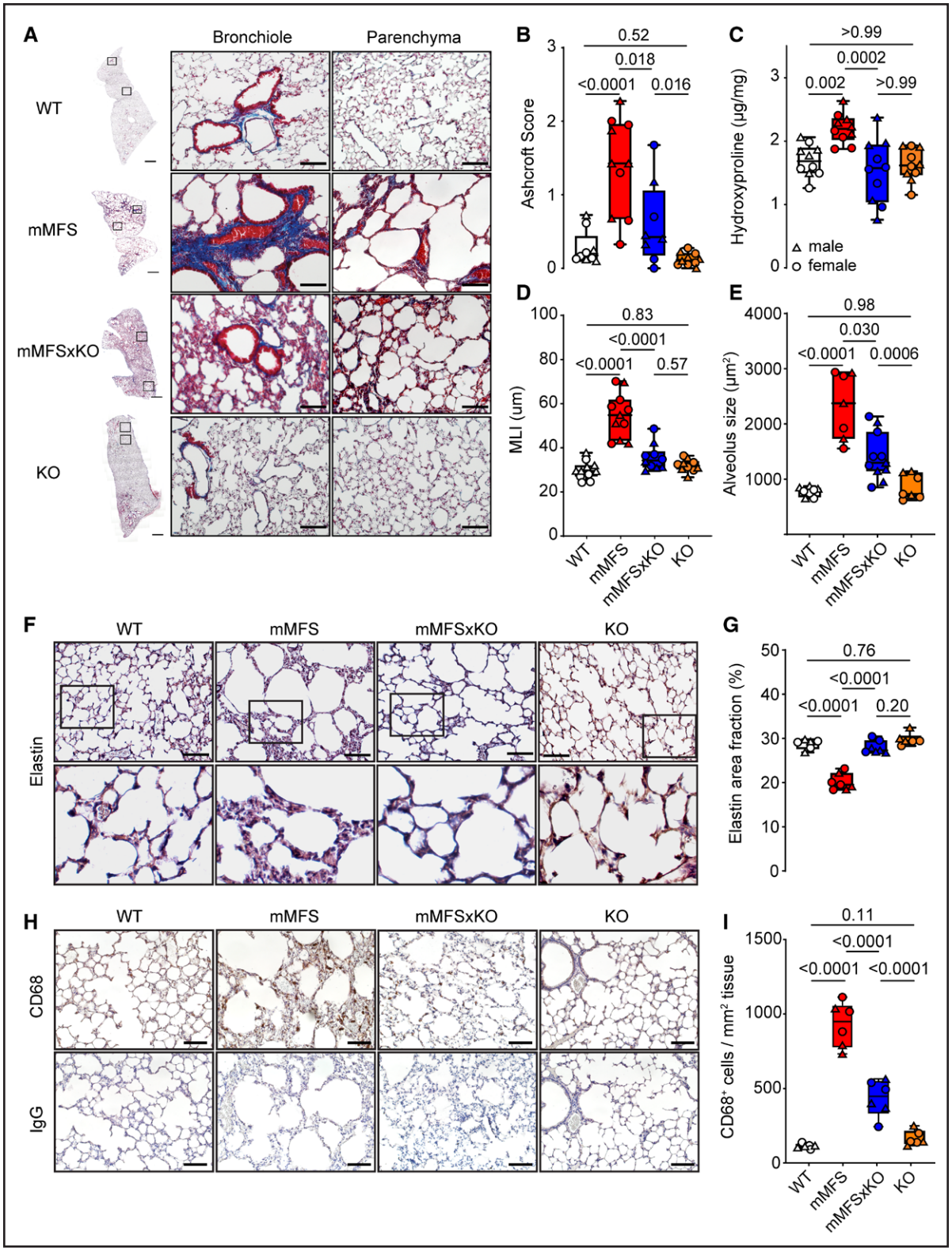

Figure 3. Lack of IL11 (interleukin-11) signaling in mouse model of Marfan Syndrome (mMFS) mice protects against pulmonary fibrosis, emphysema, and elastolysis.

A, Representative Masson's trichrome (MT)-stained photomicrographs of 16-week-old mMFS lung demonstrates increased pulmonary fibrosis, airspace enlargement, and reduced elastin content, which is prevented in mMFSxKO mice. Ashcroft scoring of pulmonary fibrosis (**B**) in MT stained lung sections (WT: n=4M, 5F; mMFS and KO: n=5M, 5F; mMFSxKO: n=4M, 4F) and hydroxyproline content assessment (**C**) in WT, mMFS, mMFSxKO, and KO lungs (n=5M, 5F). One outlier was removed from WT group for Ashcroft score analyses. Quantification of airspace enlargement by mean linear intercept (MLI; **D**; WT: n=6M, 5F; mMFS: n=5M, 6F; mMFSxKO and KO: n=5M, 5F) (*Continued*)

lung histopathology was observed (Figure S3A through S3E); therefore, analyses were conducted on pooled data for sex. By gross histological analysis of Masson's trichrome-stained lungs, we observed increased collagen deposition around bronchioles and moderate thickening of alveolar walls, along with enlargement of distal airspaces in mMFS mice as compared to WT controls (Figure 3A; Figure S4A). These distortions in lung architecture were notably diminished in mMFSxKO mice (Figure 3A; Figure S4A).

We quantified the degree of pulmonary fibrosis by 2 methods: (1) semiquantitative Ashcroft score and (2) collagen content by hydroxyproline quantification. As compared to WT controls, the lungs of mMFS mice showed increased Ashcroft scores and significantly increased lung hydroxyproline content (mean±SE; Ashcroft score: 1.39±0.21 versus 0.28±0.08; $P<0.0001$; hydroxyproline: 2.20±0.07 versus 1.69±0.08 µg/mg; $P=0.0020$ respectively; Figure 3B and 3C). In mMFSxKO lungs, both lung Ashcroft scores and collagen content were statistically reduced as compared to mMFS lungs ($P=0.018$ and $P=0.0002$, respectively), which remained elevated to knockout controls by Ashcroft score ($P=0.016$) but not hydroxyproline.

We next assessed the degree of airspace enlargement/emphysema in the lungs by quantifying alveoli chord length by MLI and the mean alveolus size. MLI and alveolus size were greater in mMFS mice as compared with WT controls (both $P<0.0001$; Figure 3D and 3E). The MLI was reduced in the mMFSxKO lungs as compared with mMFS ($P<0.0001$) and indistinguishable from knockout littermates. Alveolus size was also reduced in mMFSxKO lungs as compared to mMFS mice ($P=0.030$) and was mildly elevated as compared to knockout controls ($P=0.0006$).

Elastin, the major component of the connective tissue responsible for lung elastic recoil, is fragmented and associated with reduced lung elasticity in MFS and in mMFS mice.[12,36] Verhoef-Van Gieson elastin staining of lungs revealed reduced elastin and increased fragmentation of elastin fibres with punctate appearance in distal alveoli of mMFS lungs as compared with WT controls (Figure 3F; Figure S4B). This appearance was associated with a statistically significant decrease of elastin content in the mMFS lungs as compared to WT controls ($P<0.0001$), which was restored in mMFSxKO mice to levels similar to WT and knockout controls (Figure 3F and 3G).

Pulmonary macrophages are known to contribute to elastolytic proteases, and we quantified CD68+ macrophages in the lungs. mMFS had increased CD68+ macrophage numbers that were reduced in mMFSxKO ($P<0.0001$) although CD68+ cell numbers remained slightly but statistically significantly elevated as compared to knockout lungs (Figure 3H and 3I; Figure S4C).

To study the molecular mechanisms underlying the lesser lung pathology apparent in mMFS with *Il11ra1* loss-of-function, we examined ECM (extracellular matrix)-related (*Il11, Col1a1, Col1a2, Col3a1, Fn1, Mmp2, Mmp9,* and *Mmp12*) and proinflammatory (*Il6, Tnfa, Ccl2, Ccl5, Il1a, Il1b, Cd11b,* and *Cd68*) gene expression at the pathway level. As compared to WT mice, mMFS mice had increased expression of ECM ($P=7.2\times10^{-14}$) and proinflammatory ($P=3.4\times10^{-12}$) genes, and these effects were statistically significantly reduced in mMFSxKO as compared to mMFS mice ($P=1.4\times10^{-10}$ and $P=6.9\times10^{-7}$ respectively, Figure 4A; Table S1).

We then performed western blot analysis of IL11, collagens I and III (COL1A1 and COL3A1, respectively) and key matrix metalloproteinases (MMP2, MMP9, and MMP12) in lung homogenates. This showed that, as compared with WT mice, lungs of mMFS mice had higher levels of IL11, collagens, and MMPs (Figure 4B through 4H). In mMFS lacking IL11 signaling (mMFSxKO), expression of all these factors was reduced to levels that were no different to those seen in WT or knockout controls.

We next investigated the activation (phosphorylation) status of the 2 key IL11 signaling pathways (ERK [extracellular signal regulated kinase] and STAT3),[24] which are associated with aberrant tissue remodelling and inflammation in models of acute lung injury.[37] Compared to WT mice, mMFS displayed a non-significant increase in STAT3 activation ($P=0.26$) and significant ERK1/2 activation ($P<0.0001$; Figure 4I through 4K). Interestingly, and as seen previously in other disease models,[29] inhibition of IL11 signaling in the mMFSxKO mice was associated with lesser ERK1/2 but not STAT3 activation (Figure 4I through 4K).

Therapeutic Inhibition of IL11 Signaling Reduces Lung Pathology

The IL11RA is highly expressed by fibroblasts, vascular SMCs, and epithelial cells in the lung.[38] We next investigated whether an IL11RA neutralising antibody

Figure 3 Continued. and alveolar size (**E**; WT: n=4M, 4F; mMFS and KO: n=3M, 4F; mMFSxKO: n=5M, 6F) by histological assessment. Representative photomicrographs of Verhoef-Van Geison (VVG) staining of elastic fibres in lungs (**F**) and cumulative quantification of elastin area fraction (**G**) in WT, mMFS, mMFSxKO, and KO lungs (WT and KO: n=3M, 3F; mMFS: n=3M, 4F; mMFSxKO: n=4M, 3F). Representative photomicrographs of CD68+ cell expression in lungs (**H**) and cumulative quantification of CD68+ cell expression per tissue area (**I**; n=3M, 3F). Data presented as median±IQR; whiskers denote minimum and maximum values. Sexes are indicated as symbols for males (▲) and females (●). Statistical analysis was performed by 2-way ANOVA with Sidak multiple comparisons (**B–E**, **G** and **I**) and *P* values reported for the following groups: WT vs mMFS, mMFS vs mMFSxKO, mMFSxKO vs KO, and WT vs KO, respectively. Scale bar represents 50 µm. Additional examples of biological replicates are provided in Figure S3.

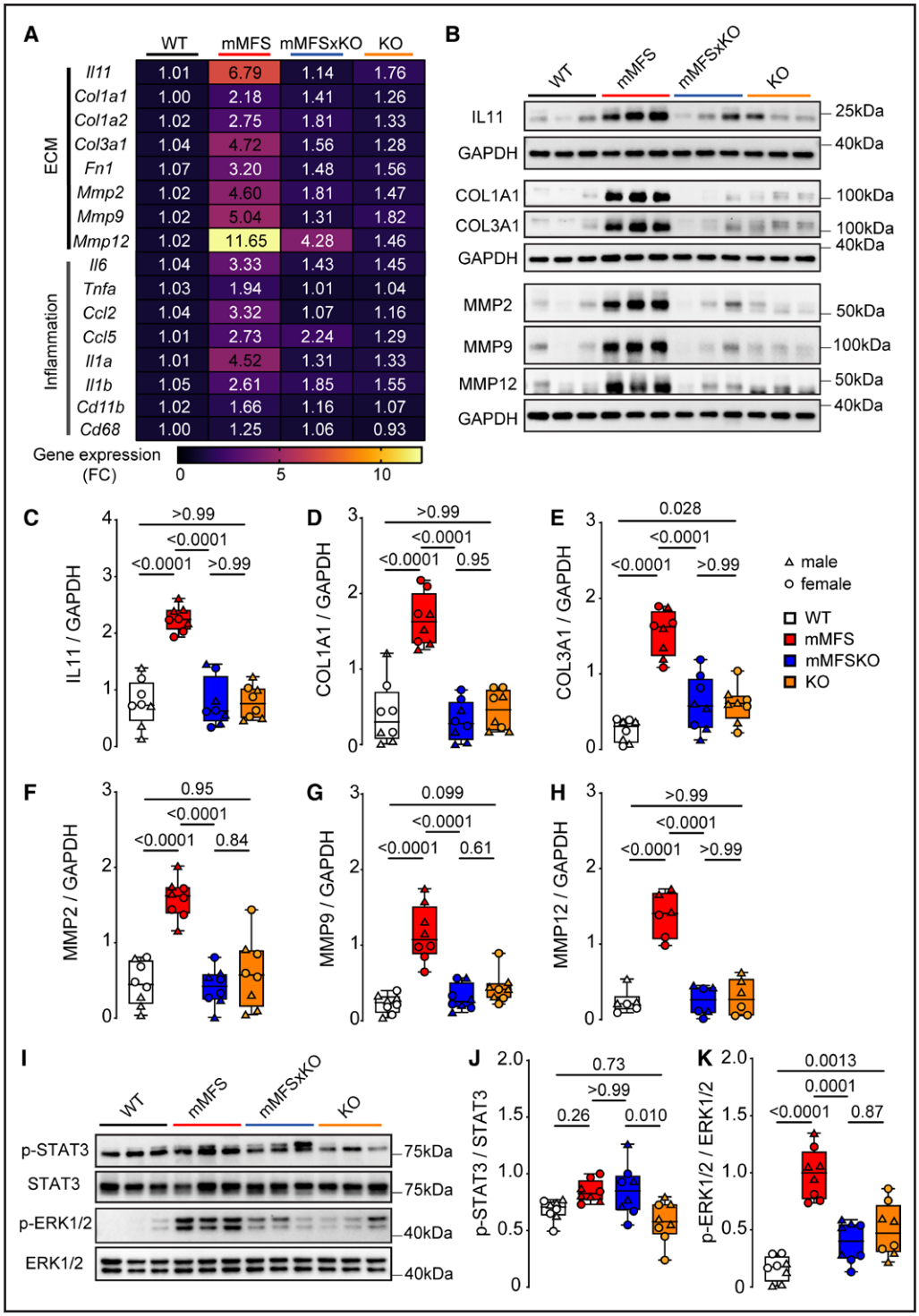

Figure 4. Lack of IL11 (interleukin-11) signaling in mouse model of Marfan Syndrome (mMFS) mice reduces pulmonary extracellular matrix modification and inflammation.

A, Heat map representation of mean gene expression, as determined by real-time polymerase chain reaction, for ECM (extracellular matrix) genes (*Il11, Col1a1, Col3a1, Fn1, Mmp2, Mmp9,* and *Mmp12*) and inflammatory genes (*Il6, Tnfa, Ccl2, Ccl5, Il1a, Il1b, Cd11b, and Cd68*) in lung lysates of 16-week-old WT, mMFS, mMFSxKO, and KO mice (n=6). Data are expressed as relative fold-change to controls with colour intensity indicating fold-change. Quantitative data are presented in Table S1. Representative immunoblots (**B**) and densitometric analyses of WT, mMFS, mMFSxKO, and KO lungs probed for IL11 (**C**), COL1A1 (**D**), COL3A1 (**E**), MMP2 (**F**), MMP9 (**G**), and MMP12 (**H**) normalized to GAPDH expression (MMP12: n=3M, 3F; others: n=4M, 4F). Representative immunoblots (**I**) and densitometry of WT, mMFS, mMFSxKO, and KO lungs probed for phosphorylated (p-) STAT3 (J) and ERK1/2 (K) normalized to their respective total expression (n=4M, 4F). Data shown are expressed as median±IQR; whiskers denote minimum and maximum values. Sexes are indicated as symbols for males (▲) and females (●). Statistical analysis was performed by 2-way ANOVA with Sidak multiple comparisons (**C–H** and **J–K**) and *P* values reported for the following groups: WT vs mMFS, mMFS vs mMFSxKO, mMFSxKO vs KO, and WT vs KO, respectively.

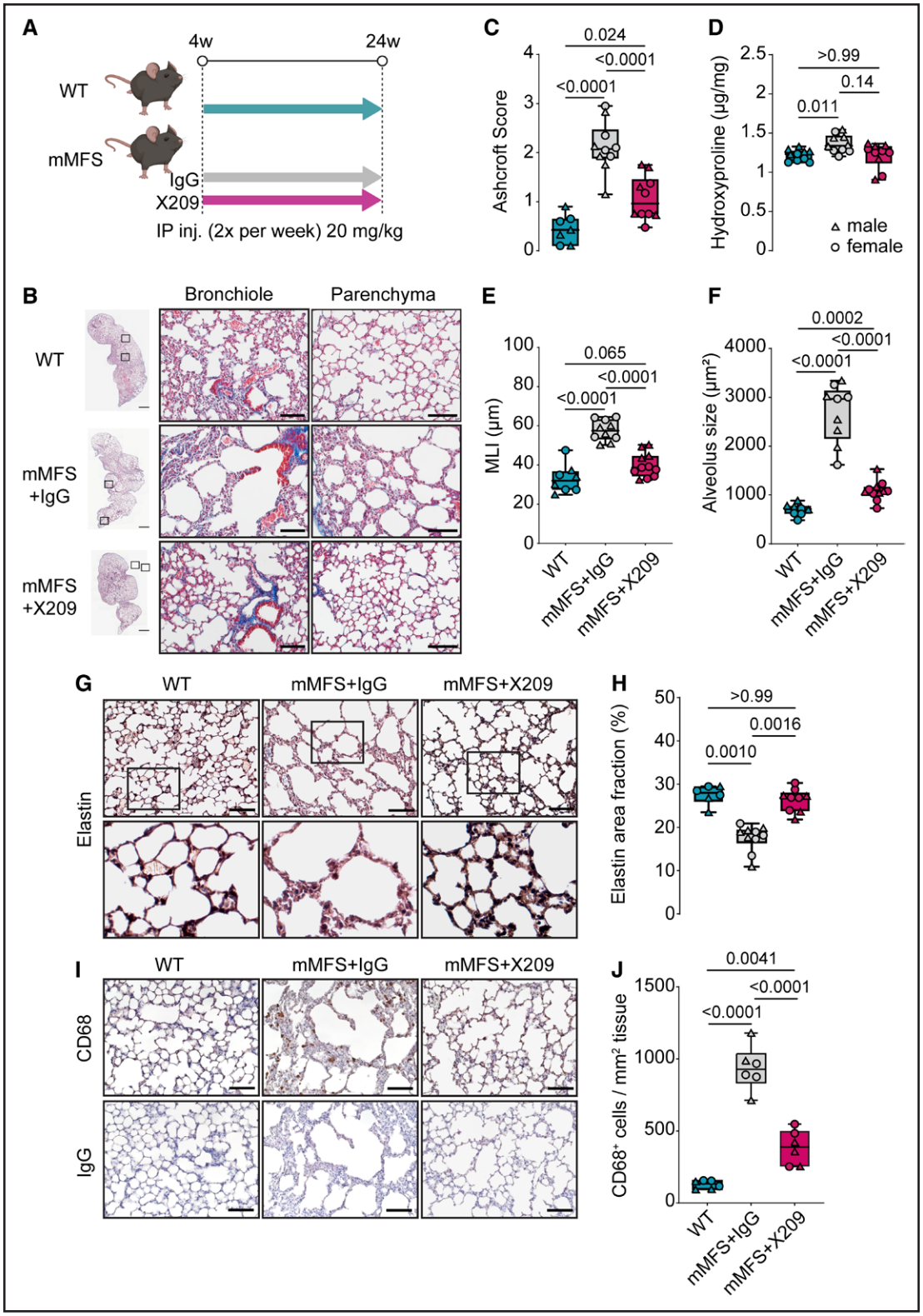

Figure 5. Therapeutic inhibition of IL11 (interleukin-11) signaling with anti-IL11RA reduces lung disease in mouse model of Marfan Syndrome (mMFS).

A, Schematic diagram of antibody therapy protocol in WT and mMFS mice. **B**, Representative Masson's trichrome (MT)-stained lung sections in 24-week-old mMFS+IgG mice demonstrates increased pulmonary fibrosis, airspace enlargement, and reduced elastin content as compared to WT mice and is partially restored with X209 treatment. Ashcroft scoring of pulmonary fibrosis (**C**) in MT-stained lung sections (WT: n=4M, 3F; mMFS+IgG and mMFS+X209: n=5M, 5F) and hydroxyproline content assessment (**D**) in lung lysates of WT, mMFS+IgG, and mMFS+X209 mice (n=5M, 5F). Quantification of airspace enlargement by mean linear intercept (MLI; **E**; WT: n=4M, 4F; (*Continued*)

(X209), which we previously characterized,[25,28,39] could reduce lung disease in mMFS mice compared with an IgG control antibody. We administered antibodies (20 mg/kg, twice per week) to mMFS mice from 4 to 24 weeks of age and compared terminal phenotypes with age-matched WT controls (Figure 5A). We have previously reported the pharmacokinetic properties of X209[28] and confirmed its bioavailability in the lungs following administration (Figure S5).

No evidence of sexual dimorphism in lung histopathology parameters was observed in the antibody-treated mMFS mice (Figure S6A through S6E), hence, analyses were conducted on pooled data for sex. By gross histology, mMFS mice treated with IgG control antibody had increased pulmonary fibrosis and emphysema as compared to WT mice and these phenotypes were markedly reduced in mMFS mice receiving anti-IL11RA (Figure 5B; Figure S7A). As expected, Ashcroft scoring and hydroxyproline assay in mMFS+IgG mice revealed increased pulmonary fibrosis as compared to WT controls (5-fold and 1.2-fold; $P<0.0001$ and $P=0.011$, respectively; Figure 5C and 5D). Similarly, indexes of emphysema by MLI and alveoli size were increased in mMFS+IgG mice as compared with WT controls (both $P<0.0001$; Figure 5E and 5F). As compared with mMFS+IgG, mMFS mice receiving anti-IL11RA from 4 to 24 weeks of age had reduced Ashcroft scores, a trend towards reduced hydroxyproline ($P=0.14$) and lesser airspace enlargement (Figure 5C through 5F). Furthermore, fragmentation of elastin fibres characterised by punctate appearance[40] and reduced elastin area fraction in the mMFS+IgG lungs was rescued in mMFS+X209 mice (Figure 5G and 5H; Figure S7B). Similarly, elevated CD68+ cell infiltration in mMFS+IgG lungs was reduced in the anti-IL11RA group ($P<0.0001$), though remaining statistically elevated as compared to WT mice (Figure 5I and 5J; Figure S7C).

To complement the molecular analyses used in our genetic studies (Figure 4), we determined the effects of therapeutic inhibition of IL11 signaling on ECM and proinflammatory gene pathways in the lungs of mice at the study end. As compared with WT mice, mMFS+IgG mice had statistically significantly increased expression of ECM related ($P=3.8\times10^{-15}$) and proinflammatory ($P=4.2\times10^{-13}$) genes and these effects were statistically significantly reduced in mMFS+X209 as compared with mMFS+IgG mice for both ECM related ($P=1.6\times10^{-13}$) and proinflammatory ($P=5.4\times10^{-10}$) genes (Figure 6A; Table S2).

Western blots of lung protein extracts showed that X209 reduced the levels of IL11, COL1A1, COL3A1, MMP2, MMP9, and MMP12 protein in mMFS lungs as compared with IgG treated mice (Figure 6B through 6H). This beneficial molecular profile was associated with lesser ERK1/2 activation but no statistically significant effect on STAT3 phosphorylation (Figure 6I through 6K).

DISCUSSION

In this study, we examined IL11 expression and functional effects in the lungs of a mouse model of MFS. In mMFS mice, we found that IL11 is upregulated in vascular SMCs, ECs, and fibroblasts and that this is associated with emphysematous changes and fibrotic remodelling of the lungs. We show that genetic or pharmacological inhibition of IL11 signaling partially reduces MFS lung pathology, which establishes a causal relationship between increased IL11 expression and pulmonary disease in MFS.

Disruption in FBN1 expression is associated with airspace enlargement and emphysematous lung disease in patients with MFS.[40] In the *Fbn1*$^{C1041G/+}$ lung, we observed fragmented elastic fibres with punctate appearance in the alveolar regions along with thicker alveolar septae. Mechanistically, the lack of functional FBN1 leads to elastin fibre fragmentation or degradation that reduces pulmonary recoil leading to enlargement of the airspace and emphysema. Additionally, elastin fragments are known to recruit inflammatory cells such as neutrophils and macrophages,[41–43] which produce elastolytic enzymes such as MMP2, MMP9, and MMP12,[44] that further exacerbate emphysematous remodeling.

Elastase-type endopeptidases, such as MMP2 and 9, causes the loss of elastic fibres in the lung in chronic obstructive pulmonary disease.[45,46] High pulmonary expression of MMP2 and 9 is also seen in apical bullae and blebs of patients with spontaneous pneumothorax[47] and bullae/blebs are seen in 10% of MFS patients and contribute to pneumothorax risk.[48] Notably, MMP2 and 9 were both elevated in the mMFS lungs in the current study and likely contribute to the elastic fiber degradation we observed. Additionally, elastase MMP12 that is predominantly secreted by alveolar macrophages and contributes to development of lung injury and emphysema,[49] was highly upregulated in mMFS lungs, and

Figure 5 Continued. mMFS+IgG: n=5M, 5F; mMFS+X209: n=5M,6F) and alveolus size (**F**; WT: n=4M, 4F; mMFS+IgG: n=5M, 4F; mMFS+X209: n=5M, 6F) under histological assessment. Representative VVG staining of elastic fibres in lung sections (**G**) and cumulative quantification of elastin area fraction (**H**; WT: n=3M, 3F; mMFS+IgG: n=5M, 5F; mMFS+X209: n=4M, 5F). Representative photomicrographs of CD68-positive cell expression in lung sections (**I**) and cumulative quantification of CD68+ cell expression per tissue area (**J**; n=3M, 3F). Data shown are expressed as median±IQR; whiskers denote minimum and maximum values. Sexes are indicated as symbols for males (▲) and females (●). Statistical analysis was performed by 1-way ANOVA with Sidak multiple comparisons (**C**, **E**, **H**, and **J**), Welch ANOVA with Dunnett post-hoc and Kruskal-Wallis with Dunn multiple comparison (**D**) for the following groups: WT vs mMFS+IgG, mMFS+IgG vs mMFS+X209, and WT vs mMFS+X209 respectively. Scale bar represents 50 µm. Additional examples of biological replicates are provided in Figure S6.

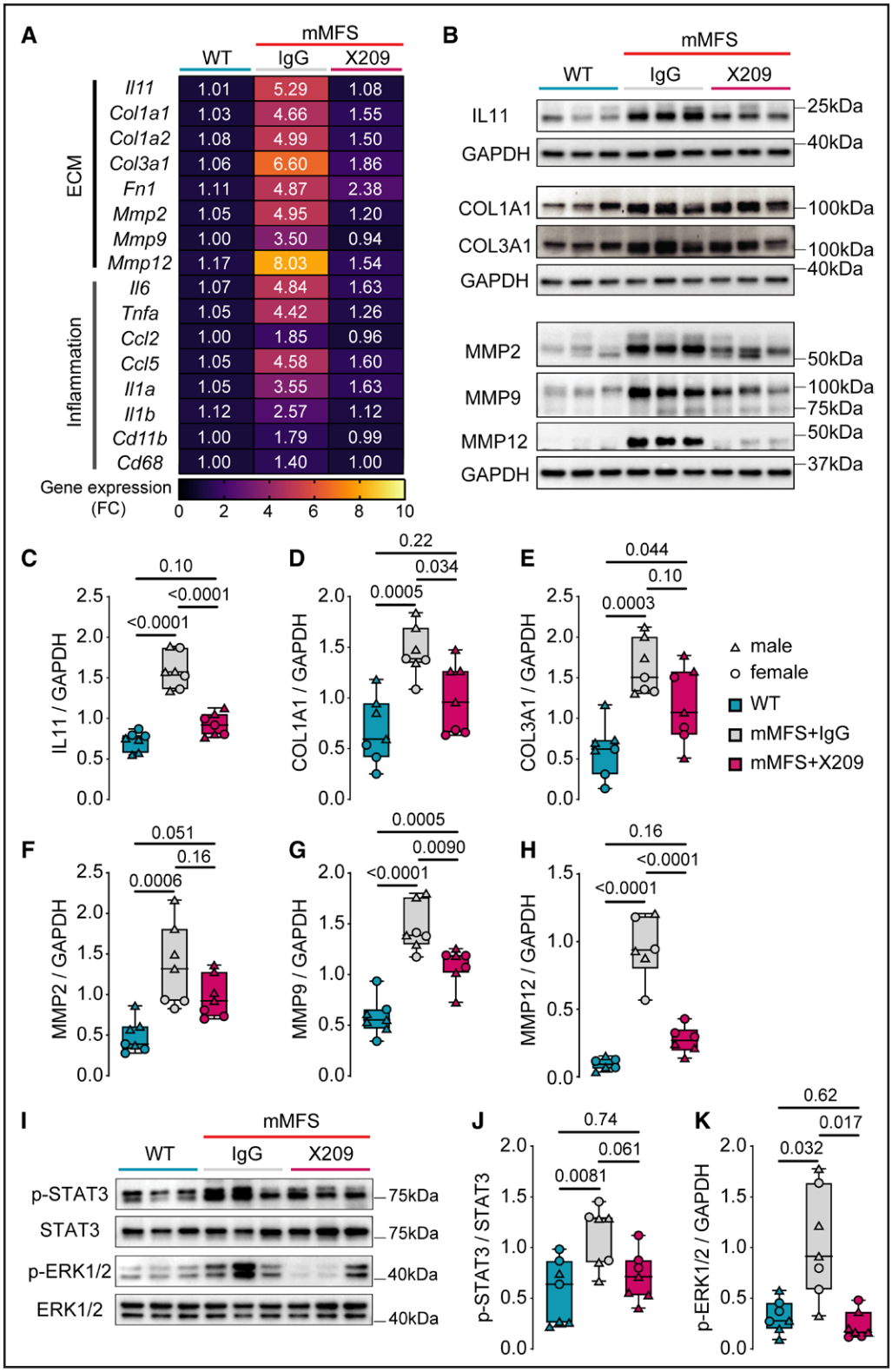

Figure 6. Therapeutic inhibition of IL11 (interleukin-11) signaling with anti-IL11RA reduces molecular pathology in mouse model of Marfan Syndrome (mMFS) lungs.

A, Heat map representation of mean gene expression, as determined by real-time polymerase chain reaction, for ECM (extracellular matrix) genes (*Il11, Col1a1, Col3a1, Fn1, Mmp2, Mmp9*, and *Mmp12*) and inflammatory genes (*Il6, Tnfa, Ccl2, Ccl5, Il1a, Il1b, Cd11b* and *Cd68*) in lung lysates of 24-week-old WT, mMFS+IgG, mMFS+X209 mice (n=6). Data are expressed as relative fold-change to controls with color intensity indicating fold-change. Quantitative data are presented in Table S2. Representative immunoblots (**B**) and densitometric analyses of WT, mMFS+IgG, mMFS+X209 lungs probed for IL11 (C), COL1A1 (**D**), COL3A1 (**E**), MMP2 (matrix metalloproteinase 2; **F**), (*Continued*)

 Arterioscler Thromb Vasc Biol. 2023;43:739–754. DOI: 10.1161/ATVBAHA.122.318802

Figure 6 Continued. MMP9 (**G**), and MMP12 (**H**) normalized to GAPDH expression (MMP12: n=3M, 3F; others: n=4M, 3F). Representative immunoblots (**I**) and densitometric analyses of WT, mMFS+IgG, mMFS+X209 lungs probed for p-STAT3 (**J**) and p-ERK1/2 (**K**) normalized to their respective total expression (n=4M, 3F). Data shown are expressed as median±IQR; whiskers denote minimum and maximum values. Sexes are indicated as symbols for males (▲) and females (●). Statistical analysis was performed by 1-way ANOVA with Sidak multiple comparisons (**C** through **I**) and Welch ANOVA with Dunnett multiple comparison (**J**) for the following groups: WT vs mMFS+IgG, mMFS+IgG vs mMFS+X209, mMFS+X209 vs WT, respectively.

associated with increased macrophage infiltration, which was reduced by genetic or pharmacologic inhibition of IL11 signaling.

We have previously shown IL11 to be amongst the top upregulated genes in TGFβ-stimulated SMCs contributing to ERK-dependent smooth muscle cell phenotypic switching in MFS aortopathy.[25,26] Likewise, IL11 is strongly induced in TGFβ-stimulated lung fibroblasts and has strong fibrogenic and proinflammatory activities.[24,29,37,50] In fibrotic lung injury, inhibition of IL11 reduced pulmonary fibrosis and lung infiltrates of profibrotic Ly6C^{+ve} monocytes, macrophages, and neutrophils.[29,37] Consistent with the anti-inflammatory and antifibrotic effects of IL11 inhibition, we observed reduced expression of proinflammatory cytokines, CD68^{+ve} macrophages, and fibrosis-related genes in the lungs of mMFS when IL11 signaling was inhibited genetically or pharmacologically.

In mMFS lung, we found IL11 expression in smooth muscle and endothelial cells occurred prior to expression in fibroblasts and that IL11 was rarely detected in alveolar epithelial cells. These findings are consistent with a previous report suggesting that fibrillin-1 mutations in the GT-8 Marfan mouse first affect the vasculature, and smooth muscle regions of the conducting airways, before progressively affecting the alveolar connective tissue and also data showing IL11 expression in the endothelium and smooth muscle cells in fibrotic lung disease.[51,52] Taken together, these data suggest that pulmonary disease in the MFS originates in the bronchopulmonary vasculature and that IL11 plays an important role in this pathology.

Increased TGFβ signaling underlies, in part, the pulmonary pathophysiology in MFS and direct or indirect inhibition of TGFβ signaling can reduce pulmonary emphysema and improve alveolar septation in mouse

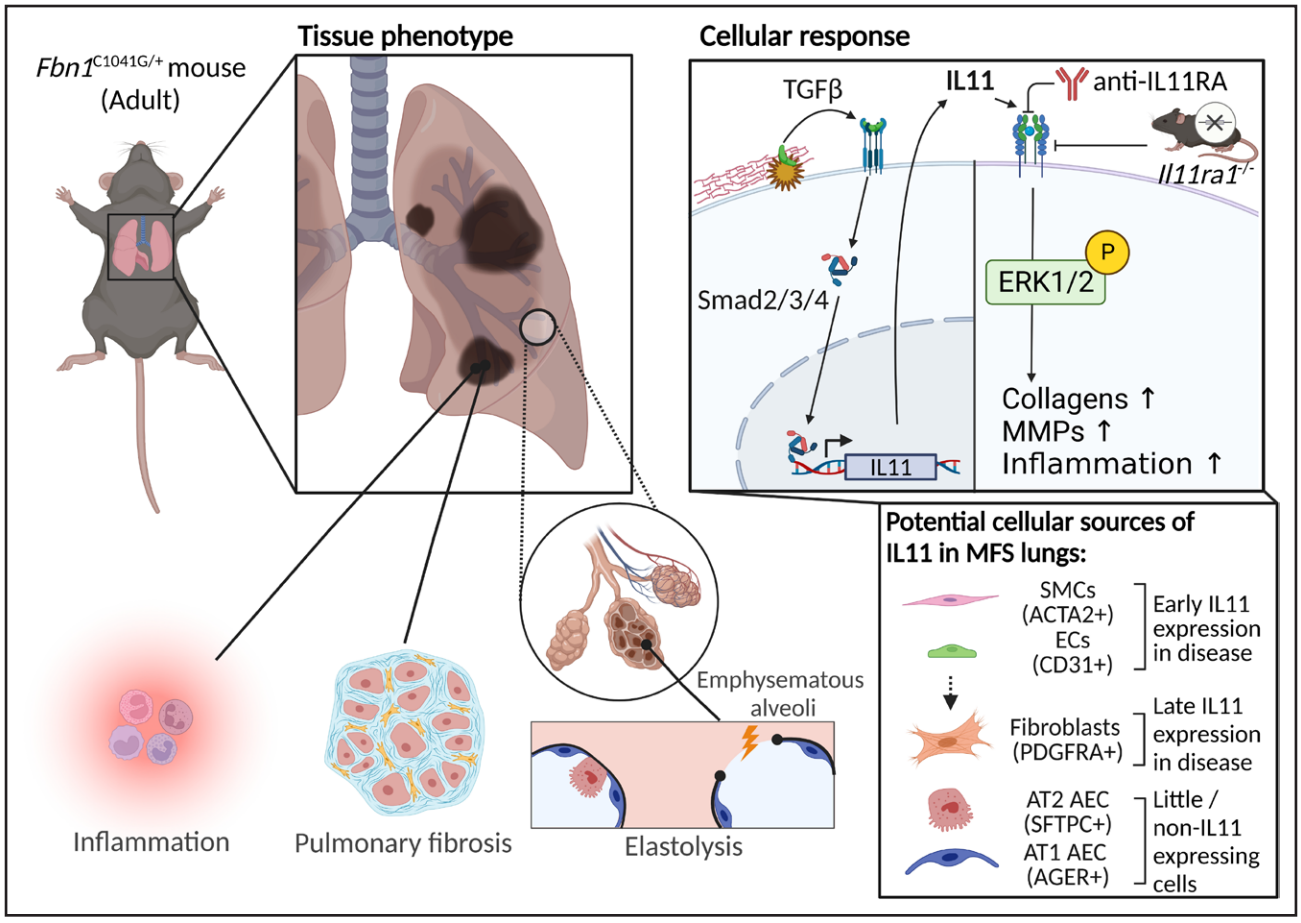

Figure 7. Schematic of the proposed association between IL11 ((interleukin-11) in Marfan syndrome associated lung pathology. Created with BioRender.com on 08/09/2022. ACTA2 indicates actin alpha 2; AGER, advanced glycosylation end-product specific receptor; PDGFRA, platelet-derived growth factor receptor alpha; SFTPC, surfactant protein C; and TGFβ, transforming growth factor beta.

models of MFS.[11,12,21,22,36,53,54] Unfortunately, due to the pleiotropic effects of TGFβ,[55,56] therapeutic inhibition of TGFβ itself is not possible in patients with MFS, or patients with other diseases, due to on-target proinflammatory toxicities.[57] Given the favorable safety profile associated with IL11 loss-of-function in mice and humans, it is possible that therapies targeting IL11 signaling offer a new therapeutic approach in MFS.[28,50,58]

There are limitations to our study. Lung function assessment was not conducted. We did not observe evidence of sexual dimorphism across MFS-associated lung pathology indices as opposed to findings in the aorta,[35] while acknowledging that sample sizes separated for sex in the current study may not be sufficiently powered to detect small effect sizes. We did not study the effects of anti-IL11RA therapy on pulmonary artery dilatation in the *Fbn1*$^{C1041G/+}$ mouse which has been previously reported to be elevated.[59] It should be noted that neither the global knockout of IL11/RA nor the treatment with anti-IL11/RA therapies are expected to alter blood pressure in mice.[23,60] Inflammatory cell infiltrates in the mMFS lung were assessed by CD68 staining for macrophages and does not detect other immune cell types such as neutrophils which are known to contribute to emphysema.

CONCLUSIONS

In conclusion, IL11 is upregulated in Marfan lung, primarily in the airways and vessels in early disease with further expression in fibroblasts, with disease progression. Therapeutic inhibition of IL11 signaling by genetic or antibody therapy protect against pulmonary emphysematous disease in a mouse model of MFS. These data show that IL11 expression causes pulmonary disease in Marfan syndrome (Figure 7). IL11 signaling was recently shown to underlie aortic disease in MFS,[25] and we suggest IL11 as a therapeutic target for treating multiorgan disease in Marfan Syndrome.

ARTICLE INFORMATION

Received September 12, 2022; accepted February 27, 2023.

Affiliations

National Heart Research Institute Singapore, National Heart Centre Singapore (B.N., C.X., L.S., X.-Y.K., D.Y., C.J.P., S.A.C., W.-W.L.). Cardiovascular and Metabolic Disorders Program, Duke-National University of Singapore Medical School (B.N., F.F.K., S.A.C., W.-W.L.). MRC-London Institute of Medical Sciences, United Kingdom (S.A.C.).

Acknowledgments

W.-W. Lim and S.A. Cook conceived and designed the study. W.-W. Lim, C. Xie, L. Su, D. Yeong, and X.-Y. Kwek maintained, bred, and genotyped the mice models. W.-W. Lim, D. Yeong, and C. Xie performed the animal experiments and organ harvests. L. Su and X.-Y. Kwek performed molecular studies. W.-W. Lim, B. Ng, C. Xie, F.F. Kuthubudeen, and D.Y. performed histological evaluations. C. Jian Pua performed the statistical analyses on gene transcription pathways. S.A. Cook provided supervision to the study. B. Ng, W.-W. Lim, and S.A. Cook drafted the article with inputs from all authors.

Sources of Funding

This work was supported by the Advanced Manufacturing and Engineering Young Individual Research Grant (AME YIRG) of Agency for Science, Technology and Research (A*STAR) award (A2084c0157 to W.-W. Lim and B. Ng), National Medical Research Council (NMRC) Singapore (NMRC/STaR/0029/2017 to S.A. Cook; NMRC-OFYIRG21jun-0022 to B. Ng), NMRC Central Grant to the NHCS (MOH-CIRG18nov-0002 to S.A. Cook), Goh Cardiovascular Research Award (Duke-NUS-GCR/2015/0014 to S.A. Cook), Tanoto Foundation (to S.A. Cook).

Disclosures

S.A. Cook is a co-inventor of the patent applications "Treatment of fibrosis" (WO/2017/103108) and "IL-11RA antibodies" (WO/2018/109170). S.A. Cook, W.W. Lim, and B. Ng are co-inventors of the patent application "Treatment of Smooth muscle cell–mediated disease" (WO/2019/073057). S.A. Cook is a co-founder and shareholder of Enleofen Bio PTE LTD, a company that develops anti-IL11 therapeutics, which were acquired for further development by Boehringer Ingelheim. All other authors declare no competing interests.

Supplemental Material

Tables S1 and S2
Figures S1–S7
Major Resources Table
Uncropped Blots
Source Data

REFERENCES

1. Dietz HC, Cutting GR, Pyeritz RE, Maslen CL, Sakai LY, Corson GM, Puffenberger EG, Hamosh A, Nanthakumar EJ, Curristin SM. Marfan syndrome caused by a recurrent de novo missense mutation in the fibrillin gene. *Nature*. 1991;352:337–339. doi: 10.1038/352337a0
2. Cañadas V, Vilacosta I, Bruna I, Fuster V. Marfan syndrome. Part 1: pathophysiology and diagnosis. *Nat Rev Cardiol*. 2010;7:256–265. doi: 10.1038/nrcardio.2010.30
3. Mecham RP. Elastin in lung development and disease pathogenesis. *Matrix Biol*. 2018;73:6–20. doi: 10.1016/j.matbio.2018.01.005
4. Dominguez R, Weisgrau RA, Santamaria M. Pulmonary hyperinflation and emphysema in infants with the Marfan syndrome. *Pediatr Radiol*. 1987;17:365–369. doi: 10.1007/BF02396609
5. Pyeritz RE. Marfan syndrome: improved clinical history results in expanded natural history. *Genet Med*. 2019;21:1683–1690. doi: 10.1038/s41436-018-0399-4
6. Child AH, Simonds AK. Pulmonary manifestations of Marfan syndrome. In Child AH (Ed.), *Diagnosis and Management of Marfan Syndrome*. 2016. Springer,
7. Dyhdalo K, Farver C. Pulmonary histologic changes in Marfan syndrome: a case series and literature review. *Am J Clin Pathol*. 2011;136:857–863. doi: 10.1309/AJCP79SNDHGKQFIN
8. Corsico AG, Grosso A, Tripon B, Albicini F, Gini E, Mazzetta A, Di Vincenzo EM, Agnesi ME, Tsana Tegomo E, Ronzoni V, et alPulmonary involvement in patients with Marfan syndrome. *Panminerva Med*. 2014;56:177–182.
9. Carta L, Pereira L, Arteaga-Solis E, Lee-Arteaga SY, Lenart B, Starcher B, Merkel CA, Sukoyan M, Kerkis A, Hazeki N, et alFibrillins 1 and 2 perform partially overlapping functions during aortic development. *J Biol Chem*. 2006;281:8016–8023. doi: 10.1074/jbc.M511599200
10. Pereira L, Andrikopoulos K, Tian J, Lee SY, Keene DR, Ono R, Reinhardt DP, Sakai LY, Biery NJ, Bunton T, et alTargetting of the gene encoding fibrillin-1 recapitulates the vascular aspect of Marfan syndrome. *Nat Genet*. 1997;17:218–222. doi: 10.1038/ng1097-218
11. Neptune ER, Frischmeyer PA, Arking DE, Myers L, Bunton TE, Gayraud B, Ramirez F, Sakai LY, Dietz HC. Dysregulation of TGF-β activation contributes to pathogenesis in Marfan syndrome. *Nat Genet*. 2003;33:407–411. doi: 10.1038/ng1116
12. Lee JJ, Galatioto J, Rao S, Ramirez F, Costa KD. Losartan attenuates degradation of aorta and lung tissue micromechanics in a mouse model of severe Marfan syndrome. *Ann Biomed Eng*. 2016;44:2994–3006. doi: 10.1007/s10439-016-1616-4
13. Pereira L, Lee SY, Gayraud B, Andrikopoulos K, Shapiro SD, Bunton T, Biery NJ, Dietz HC, Sakai LY, Ramirez F. Pathogenetic sequence for aneurysm revealed in mice underexpressing fibrillin-1. *Proc Natl Acad Sci U S A*. 1999;96:3819–3823. doi: 10.1073/pnas.96.7.3819

14. Chaudhry SS, Cain SA, Morgan A, Dallas SL, Shuttleworth CA, Kielty CM. Fibrillin-1 regulates the bioavailability of TGFbeta1. *J Cell Biol*. 2007;176:355–367. doi: 10.1083/jcb.200608167
15. Holm TM, Habashi JP, Doyle JJ, Bedja D, Chen Y, van Erp C, Lindsay ME, Kim D, Schoenhoff F, Cohn RD, et alNoncanonical TGFbeta signaling contributes to aortic aneurysm progression in Marfan syndrome mice. *Science*. 2011;332:358–361. doi: 10.1126/science.1192149
16. Judge DP, Biery NJ, Keene DR, Geubtner J, Myers L, Huso DL, Sakai LY, Dietz HC. Evidence for a critical contribution of haploinsufficiency in the complex pathogenesis of Marfan syndrome. *J Clin Invest*. 2004;114:172–181. doi: 10.1172/JCI20641
17. Uriarte JJ, Meirelles T, del Blanco DG, Nonaka PN, Campillo N, Sarri E, Navajas D, Egea G, Farré R. Early Impairment of lung mechanics in a Murine model of Marfan syndrome. *PLoS One*. 2016;11:e0152124. doi: 10.1371/journal.pone.0152124
18. Xiong W, Knispel RA, Dietz HC, Ramirez F, Baxter BT. Doxycycline delays aneurysm rupture in a mouse model of Marfan syndrome. *J Vasc Surg*. 2008;47:166–172; discussion 172. doi: 10.1016/j.jvs.2007.09.016
19. Chung AWY, Yang HHC, Radomski MW, van Breemen C. Long-term doxycycline is more effective than atenolol to prevent thoracic aortic aneurysm in marfan syndrome through the inhibition of matrix metalloproteinase-2 and -9. *Circ Res*. 2008;102:e73–e85. doi: e10.1161/CIRCRESAHA.108.174367
20. Chakrabarti S, Patel KD. Matrix metalloproteinase-2 (MMP-2) and MMP-9 in pulmonary pathology. *Exp Lung Res*. 2005;31:599–621. doi: 10.1080/019021490944232
21. Habashi JP, Judge DP, Holm TM, Cohn RD, Loeys BL, Cooper TK, Myers L, Klein EC, Liu G, Calvi C, et alLosartan, an AT1 antagonist, prevents aortic aneurysm in a mouse model of Marfan syndrome. *Science*. 2006;312:117–121. doi: 10.1126/science.1124287
22. Habashi JP, Doyle JJ, Holm TM, Aziz H, Schoenhoff F, Bedja D, Chen Y, Modiri AN, Judge DP, Dietz HC. Angiotensin II type 2 receptor signaling attenuates aortic aneurysm in mice through ERK antagonism. *Science*. 2011;332:361–365. doi: 10.1126/science.1192152
23. Schafer S, Viswanathan S, Widjaja AA, Lim W-W, , Moreno-Moral A, DeLaughter DM, Ng B, Patone G, Chow K, et alIL-11 is a crucial determinant of cardiovascular fibrosis. *Nature*. 2017;552:110–115. doi: 10.1038/nature24676
24. Widjaja AA, Chothani S, Viswanathan S, Goh JWT, Lim WW, Cook SA. IL11 stimulates IL33 expression and proinflammatory fibroblast activation across tissues. *Int J Mol Sci* . 2022;23:8900. doi: 10.3390/ijms23168900
25. Lim WW, Dong J, Ng B, Widjaja AA, Xie C, Su L, Kwek X-Y, , Tee NGZ, , et alInhibition of IL11 signaling reduces aortic pathology in murine marfan syndrome. *Circ Res*. 2022;130:728–740. doi: 10.1161/CIRCRESAHA.121.320381
26. Lim WW, Corden B, Ng B, Vanezis K, D'Agostino G, Widjaja AA, Song W-H, , Xie C, Su L, et al. Interleukin-11 is important for vascular smooth muscle phenotypic switching and aortic inflammation, fibrosis and remodeling in mouse models. *Sci Rep*. 2020;10:17853. doi: 10.1038/s41598-020-74944-7
27. Widjaja AA, Dong J, Adami E, Viswanathan S, Ng B, Pakkiri LS, Chothani SP, Singh BK, Lim WW, , et al. Redefining IL11 as a regeneration-limiting hepatotoxin and therapeutic target in acetaminophen-induced liver injury. *Sci Transl Med*. 2021;13:eaba8146. doi: 10.1126/scitranslmed.aba8146
28. Widjaja AA, Singh BK, Adami E, Viswanathan S, Dong J, D'Agostino GA, Ng B, Lim WW, , Tan J, et al. Inhibiting interleukin 11 signaling reduces hepatocyte death and liver fibrosis, inflammation, and steatosis in mouse models of nonalcoholic steatohepatitis. *Gastroenterology*. 2019;157:777–792.e14. doi: 10.1053/j.gastro.2019.05.002
29. Ng B, Dong J, D'Agostino G, Viswanathan S, Widjaja AA, Lim W-W, Ko NSJ, , Tan J, et alInterleukin-11 is a therapeutic target in idiopathic pulmonary fibrosis. *Sci Transl Med*. 2019;11:eaaw1237. doi: 10.1126/scitranslmed.aaw1237
30. Lim WW, Ng B, Widjaja A, Xie C, Su L, Ko N, Lim S-Y, , Kwek X-Y, , et al. Transgenic interleukin 11 expression causes cross-tissue fibroinflammation and an inflammatory bowel phenotype in mice. *PLoS One*. 2020;15:e0227505. doi: 10.1371/journal.pone.0227505
31. Salaets T, Tack B, Gie A, Pavie B, Sindhwani N, Jimenez J, Regin Y, Allegaert K, Deprest J, Toelen J. A semi-automated method for unbiased alveolar morphometry: Validation in a bronchopulmonary dysplasia model. *PLoS One*. 2020;15:e0239562. doi: 10.1371/journal.pone.0239562
32. Wang C, de Mochel NSR, Christenson SA, Cassandras M, Moon R, Brumwell AN, Byrnes LE, Li A, Yokosaki Y, Shan P, et al. Expansion of hedgehog disrupts mesenchymal identity and induces emphysema phenotype. *J Clin Invest*. 2018;128:4343–4358. doi: 10.1172/JCI99435
33. Machado MN, Mazzoli-Rocha F, Casquilho NV, Maron-Gutierrez T, Ortenzi VH, Morales MM, Fortunato RS, Zin WA. Bone marrow-derived mononuclear cell therapy in papain-induced experimental pulmonary emphysema. *Front Physiol*. 2018;9:121. doi: 10.3389/fphys.2018.00121
34. Oliveira MV, Abreu SC, Padilha GA, Rocha NN, Maia LA, Takiya CM, Xisto DG, Suki B, Silva PL, Rocco PRM, et al. Characterization of a mouse model of emphysema induced by multiple instillations of low-dose elastase. *Front Physiol*. 2016;7:457. doi: 10.3389/fphys.2016.00457
35. Chen JZ, Sawada H, Ye D, Katsumata Y, Kukida M, Ohno-Urabe S, Moorleghen JJ, Franklin MK, Howatt DA, Sheppard MB, et al. Deletion of AT1a (Angiotensin II Type 1a) receptor or inhibition of angiotensinogen synthesis attenuates thoracic aortopathies in fibrillin1 mice. *Arterioscler Thromb Vasc Biol*. 2021;41:2538–2550. doi: 10.1161/ATVBAHA.121.315715
36. Jespersen K, Liu Z, Li C, Harding P, Sestak K, Batra R, Stephenson CA, Foley RT, Greene H, Meisinger T, et al. Enhanced Notch3 signaling contributes to pulmonary emphysema in a Murine Model of Marfan syndrome. *Sci Rep*. 2020;10:10949. doi: 10.1038/s41598-020-67941-3
37. Ng B, Dong J, Viswanathan S, Widjaja AA, Paleja BS, Adami E, Ko NSJ, , Wang M, Lim S, et al. Fibroblast-specific IL11 signaling drives chronic inflammation in murine fibrotic lung disease. *FASEB J*. 2020;34:11802–11815. doi: 10.1096/fj.202001045RR
38. Ng B, Cook SA, Schafer S. Interleukin-11 signaling underlies fibrosis, parenchymal dysfunction, and chronic inflammation of the airway. *Exp Mol Med*. 2020;52:1871–1878. doi: 10.1038/s12276-020-00531-5
39. Lim W, Corden B, Ye L, Viswanathan S, Widjaja AA, Xie C, Su L, Tee NGZ, , Schafer S, et al. Antibody-mediated neutralization of IL11 signalling reduces ERK activation and cardiac fibrosis in a mouse model of severe pressure overload. *Clin Exp Pharmacol Physiol*. 2021;48:605–613. doi: 10.1111/1440-1681.13458
40. Robbesom AA, Koenders MMJ, Smits NC, Hafmans T, Versteeg EMM, Bulten J, Veerkamp JH, Richard Dekhuijzen PN, van Kuppevelt TH. Aberrant fibrillin-1 expression in early emphysematous human lung: a proposed predisposition for emphysema. *Mod Pathol*. 2008;21:297–307. doi: 10.1038/modpathol.3801004
41. Margaroli C, Madison MC, Viera L, Russell DW, Gaggar A, Genschmer KR, Blalock JE. An in vivo model for extracellular vesicle-induced emphysema. *JCI Insight*. 2022;7:e153560. doi: 10.1172/jci.insight.153560
42. Houghton AM, Quintero PA, Perkins DL, Kobayashi DK, Kelley DG, Marconcini LA, Mecham RP, Senior RM, Shapiro SD. Elastin fragments drive disease progression in a murine model of emphysema. *J Clin Invest*. 2006;116:753–759. doi: 10.1172/JCI25617
43. Shapiro SD, Goldstein NM, Houghton AM, Kobayashi DK, Kelley D, Belaaouaj A. Neutrophil elastase contributes to cigarette smoke-induced emphysema in mice. *Am J Pathol*. 2003;163:2329–2335. doi: 10.1016/S0002-9440(10)63589-4
44. Sellami M, Meghraoui-Kheddar A, Terryn C, Fichel C, Bouland N, Diebold MD, Guenounou M, Héry-Huynh S, Le Naour R. Induction and regulation of murine emphysema by elastin peptides. *Am J Physiol Lung Cell Mol Physiol*. 2016;310:L8–L23. doi: 10.1152/ajplung.00068.2015
45. Ohnishi K, Takagi M, Kurokawa Y, Satomi S, Konttinen YT. Matrix metalloproteinase-mediated extracellular matrix protein degradation in human pulmonary emphysema. *Lab Invest*. 1998;78:1077–1087.
46. Segura-Valdez L, Pardo A, Gaxiola M, Uhal BD, Becerril C, Selman M. Upregulation of gelatinases A and B, collagenases 1 and 2, and increased parenchymal cell death in COPD. *Chest*. 2000;117:684–694. doi: 10.1378/chest.117.3.684
47. Chen CK, Chen PR, Huang HC, Lin YS, Fang HY. Overexpression of matrix metalloproteinases in lung tissue of patients with primary spontaneous pneumothorax. *Respiration*. 2014;88:418–425. doi: 10.1159/000366065
48. Karpman C, Aughenbaugh GL, Ryu JH. Pneumothorax and bullae in Marfan syndrome. *Respiration*. 2011;82:219–224. doi: 10.1159/000322958
49. Spix B, Butz ES, Chen CC, Rosato AS, , Tang R, Jeridi A, Kudrina V, Plesch E, Wartenberg P, et alLung emphysema and impaired macrophage elastase clearance in mucolipin 3 deficient mice. *Nat Commun*. 2022;13:318. doi: 10.1038/s41467-021-27860-x
50. Ng B, Widjaja AA, Viswanathan S, Dong J, Chothani SP, Lim S, Shekeran SG, Tan J, McGregor NE, Walker EC, et al. Similarities and differences between IL11 and IL11RA1 knockout mice for lung fibro-inflammation, fertility and craniosynostosis. *Sci Rep*. 2021;11:14088. doi: 10.1038/s41598-021-93623-9
51. Charbonneau NL, Manalo EC, Tufa SF, Carlson EJ, Carlberg VM, Keene DR, Sakai LY. Fibrillin-1 in the vasculature: in vivo accumulation of eGFP-tagged fibrillin-1 in a knockin mouse model. *Anat Rec*. 2020;303:1590–1603. doi: 10.1002/ar.24217

52. Milara J, Roger I, Montero P, Artigues E, Escrivá J, Cortijo J. IL-11 system participates in pulmonary artery remodeling and hypertension in pulmonary fibrosis. *Respir Res.* 2022;23:313. doi: 10.1186/s12931-022-02241-0
53. Guo G, Muñoz-García B, Ott CE, Grünhagen J, Mousa SA, Pletschacher A, von Kodolitsch Y, Knaus P, Robinson PN. Antagonism of GxxPG fragments ameliorates manifestations of aortic disease in Marfan syndrome mice. *Hum Mol Genet.* 2013;22:433–443. doi: 10.1093/hmg/dds439
54. Vera L, Garcia-Olloqui P, Petri E, Viñado AC, , Valera PS, Blasco-Iturri Z, Calvo IA, Cenzano I, Ruppert C, et alNotch3 deficiency attenuates pulmonary fibrosis and impedes lung-function decline. *Am J Respir Cell Mol Biol.* 2021;64:465–476. doi: 10.1165/rcmb.2020-0516OC
55. Cook JR, Clayton NP, Carta L, Galatioto J, Chiu E, Smaldone S, Nelson CA, Cheng SH, Wentworth BM, Ramirez F. Dimorphic effects of transforming growth factor-β signaling during aortic aneurysm progression in mice suggest a combinatorial therapy for Marfan syndrome. *Arterioscler Thromb Vasc Biol.* 2015;35:911–917. doi: 10.1161/ATVBAHA.114.305150
56. Kotlarz D, Marquardt B, Barøy T, Lee WS, Konnikova L, Hollizeck S, Magg T, Lehle AS, Walz C, Borggraefe I, et alHuman TGF-β1 deficiency causes severe inflammatory bowel disease and encephalopathy. *Nat Genet.* 2018;50:344–348. doi: 10.1038/s41588-018-0063-6
57. Voelker J, Berg PH, Sheetz M, Duffin K, Shen T, Moser B, Greene T, Blumenthal SS, Rychlik I, Yagil Y, et alAnti-TGF-β1 antibody therapy in patients with diabetic nephropathy. *J Am Soc Nephrol.* 2017;28:953–962. doi: 10.1681/ASN.2015111230
58. Cook SA, Schafer S. Hiding in plain sight: interleukin-11 emerges as a master regulator of fibrosis, tissue integrity, and stromal inflammation. *Annu Rev Med.* 2020;71:263–276. doi: 10.1146/annurev-med-041818-011649
59. White Z, Milad N, Tehrani AY, Lamothe J, Hogg JC, Esfandiarei M, Seidman M, Booth S, Hackett T-L, , et al. Sildenafil prevents marfan-associated emphysema and early pulmonary artery dilation in mice. *Am J Pathol.* 2019;189:1536–1546. doi: 10.1016/j.ajpath.2019.05.003
60. Guo Y, Lu Y, Lu X, He S, Li S-J, , Shao S, Zhou H-D, , Wang R-Q, et al. Krüppel-like factor 15/interleukin 11 axis-mediated adventitial remodeling depends on extracellular signal-regulated Kinases 1 and 2 activation in Angiotensin ii–induced hypertension. *J Am Heart Assoc.* 2021;10:e020554. doi: 10.1161/JAHA.120.020554